RSC Advances

RSC Advances

www.rsc.org/advances

ROYAL SOCIETY OF CHEMISTRY

www.rsc.org/advances

Graphical Abstract:

Two new inorganic-organic hybrid materials based on polyhedral oligomeric silsesquioxane (POSS) capped with an emissive Ir(III) complex and carbazole units were successfully synthesized and characterized. The photophysical and electrochemical characterization, and thermal stabilities of two inorganic/organic hybrid materials were investigated detailedly. Solution processed light-emitting devices based on the POSS materials exhibited ultrahigh brightness and higher external quantum efficiency.
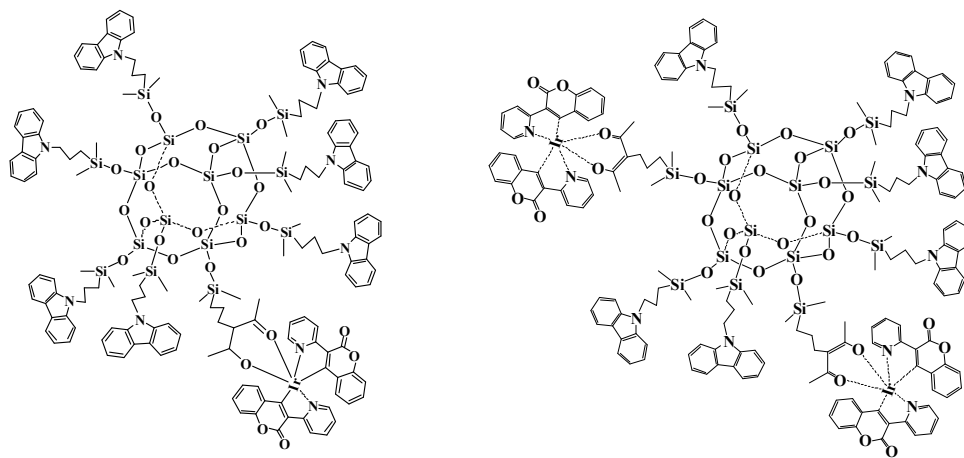
Synthesis and Photo- and Electro-luminescent Properties of Ir(III) Complexes Attached Polyhedral Oligomeric Silsesquioxane Materials

Tianzhi Yu[1,*], Xin Wang[1], Wenming Su[2,*], Chengcheng Zhang[1], Yuling Zhao[3], Hui Zhang[1], Zixuan Xu[1]

[1]Key Laboratory of Opto-Electronic Technology and Intelligent Control (Ministry of Education), Lanzhou Jiaotong University, Lanzhou 730070, China

[2]Printable electronics research center, Suzhou Institute of Nano-Tech and Nano-Bionics, Chinese Academy of Sciences, Suzhou 215123, China

[3]School of Chemical and Biological Engineering, Lanzhou Jiaotong University, Lanzhou 730070, China

Abstract: This paper describes synthesis, photophysical, electrochemical characterizations of two new polyhedral oligomeric silsesquioxane (POSS)-basded green-light phosphorescent materials, consisting of an emissive Ir(III) complex and carbazole moieties covalently attached to a polyhedral oligomeric silsesquioxane (POSS) core. These phosphorescent POSS materials offer many advantages including amorphous properties, good thermal stabilities, and good solubility in common solvents, and high purity via column chromatography. The photoluminescence spectra of the POSS materials in solutions and in the solid states indicate a reduction in the degrees of interactions among Ir(III) complex units and concentration quenching due to the bulky POSS core. Solution processed light-emitting devices with a configuration of ITO/PEDOT:PSS (45 nm)/CBP: POSS materials (50

---

[*] Corresponding Author. Tel. +86-931-4956935; Fax: +86-931-4938756; e-mail: yutianzhi@hotmail.com (T.Z. Yu); wmsu2008@sinano.ac.cn (W.M. Su).

nm)/TPBi (50 nm)/Liq (2 nm)/Al(150 nm) were fabricated. The devices based on these POSS

materials exhibit maximum external quantum efficiency (EQE) of 7.82% and a maximum luminance

of 21285 cd/m^2.

Keywords: Iridium complex; POSS; Photoluminescence; Electroluminescence

1. Introduction

Phosphorescent heavy-metal complexes as emitters in organic light-emitting diodes (OLEDs)

have attracted tremendous attention because they can fully utilize both singlet and triplet excitons

through the strong spin-orbital coupling of heavy-metal ions [1-4]. Among those phosphorescent

materials, iridium complexes are the most valuable emitting materials due to their high quantum

efficiency, brightness, color diversity, short excited-state lifetime and good thermal stability, which

make them an attractive alternative for optoelectronic applications including OLEDs, light-emitting

electrochemical cells, chemosensors and biological labeling [5-10]. Over the past several years,

considerable efforts have been devoted to the exploitation of novel Ir(III) complexes for highly

efficient OLEDs. Upon to now, blue, green, yellow, orange and red emitting Ir(III) complexes have

been developed by the design and synthesis of cyclometalating ligands or by modulating the

ancillary ligands [3,4,6,11,12]. However, the Ir(III) complexes used as EL materials are suffering from

self-quenching in solid state due to interaction and aggregation with its neighboring complexes.

Introducing steric hindrance or bulky side groups into Ir(III) complexes is an effective strategy to

suppress the emission quenching and enhance the device performance [7,12-14].

Polyhedral oligomeric silsesquioxane (POSS) unit is a cube-shaped nanoparticle in which the

rigid silica-like inorganic core can be attached with eight organic functional groups at its silicon

vertices [15,16]. POSS has attracted considerable interest in materials science due to its well-defined

nano-scale organic-inorganic structure, which makes it an ideal building block for constructing

nano-structured hybrid materials and nanocomposites [17-19]. POSS macromolecules can be easily

synthesized to be monofunctional or multifunctional materials for commercial applications by

grafting with organic functional groups. Moreover, POSS macromolecules attaching the

carrier-transporting moieties and/or chromophores can provide the advantages of both small

molecule and polymer light-emitting materials including high purity and solution processability

[20,21]. The incorporation of POSS into organic light emitting materials has led to significant

improvements in the performance of organic light emitting devises (OLEDs). Since the first use of

POSS as central cores for solution processed hybrid hole transport materials in OLEDs that

enhanced brightness and efficiencies as compared to the devices that used traditional hole transport

materials [22], the POSS functionalized light emitting materials were widely used in OLEDs. The

Heeger group pioneered the use of POSS-based light emitting polymers in which POSS cores as

end-cappers   were   attached   at   the   chain   ends   of

poly[2-methoxy-5-(2-ethylhexyloxy)-1,4-phenylenevinylene]   (MEH-PPV)   and

poly(9,9′-dioctylfluorene) [23]. The electroluminescent device made from the POSS-capped

MEH-PPV polymer was found to exhibit higher brightness (1320 cd/m^2 at 3.5V) and external

quantum efficiency (EQE) (η_{ext} = 2.2%) than the POSS-free MEH-PPV (230 cd/m^2 at 3.5 V and η_{ext}

= 1.5%). The enhanced device properties may be attributed to reduced aggregation caused by the

bulky POSS end groups and improved adhesion of the polymer to the ITO coated glass substrate.

Thereafter, some research groups reported the photoluminescence and electroluminescence

properties of POSS-functionalized polyfluorene materials in which POSS units were appended to the

polyfluorene backbone using an alkoxy spacer [24,25]. These POSS-functionalized polyfluorene materials showed higher fluorescence quantum yields and better thermal stability than the corresponding pristine polymers because the inorganic POSS units strongly suppressed intermolecular aggregation and/or thermal oxidation and crosslinking. Recently, research on phosphorescent emitters and efficient light-emitting devices based on POSS materials have also attracted tremendous interest [21,26,27]. Yang et al. [21] reported efficient monochromatic and white-emitting OLEDs utilizing Ir(III) complex-functionalized POSS materials, in which the monochromatic OLEDs exhibited maximum external quantum efficiencies in the range of 5–9% and maximum brightness of 1000 cd/m^2, and the white-emitting OLEDs shown EQEs of 8.0%, power efficiencies of 8.1 lm/W, and CIE coordinates of (0.36, 0.39) at 1000 cd/m^2. Singh et al. [27] reported the inkjet printing OLEDs based on Ir(III) complex-functionalized POSS meterials, the devices exhibited peak luminances of ~ 10000 cd/m^2 with peak quantum efficiencies of ~ 2.5%.

The cyclometalated Ir(III) coumarin complexes have been investigated detailedly in our laboratory, which exhibited good photo- and electro-luminescence properties [28]. In this paper, we first used 3-allylpentane-2,4-dione (acac-allyl) as the ancillary ligand to synthesize a new iridium(III) coumarin complex, Ir(L)$_2$(acac-allyl), which was as an emissive iridium complex. Then two new Ir(III) complex-functionalized POSS meterials, 7Cz-Ir(L)$_2$(acac)-POSS and 6Cz-2Ir(L)$_2$(acac)-POSS, consisting of one or two emissive iridium(III) complexes and carbazole moieties covalently attached to a polyhedral oligomeric silsesquioxane (POSS) core were successfully synthesized and characterized. The photophysical properties and thermal stability of these POSS materials were investigated. Furthermore, solution processed light-emitting devices based on these POSS materials were fabricated to investigate the electroluminescence properties of the POSS materials.

4

The synthetic routes of 7Cz-Ir(L)$_2$(acac)-POSS and 6Cz-2Ir(L)$_2$(acac)-POSS were shown in Scheme 1.

2. Experimental

2.1 Materials and methods

Carbazole and allyl bromide were bought from Alfa Aesar. Acetylacetone was purchased from Shanghai Jingchun Reagent Co. Ltd. (China). Platinum complex (platinum-1,3-divinyl-1,1,3,3-tetramethyldisiloxane, Pt-dvs, 2 wt% Pt in xylene) was purchased from Aldrich, USA. Octakis(dimethylsiloxy)silsesquioxane (Q$_8$M$_8$^{H}) containing eight hydro-silane groups was purchased from the Hybrid Plastics Co., USA. 8-Hydroxyquinolinolato-lithium (Liq), 4,4′-Bis(9-carbazolyl)biphenyl (CBP) and 1,3,5-Tri(N-phenylbenzimidazol-2-yl)benzene (TPBi) were purchased from Electro-Light Technology Corp., Beijing. Toluene was dried by distillation before use in the hydrosilylation reaction. All other chemicals were analytical grade reagent.

The cyclometalated coumarin ligand (3-(pyridine-2-yl)coumarin, **L**) and the cyclometalated Ir(III) μ-chlorobridged dimmer ((L)$_2$Ir(μ-Cl)$_2$Ir(L)$_2$) were prepared as previously described [29].

^{1}H NMR spectra were obtained on Unity Varian-500MHz. IR spectra (400 – 4000 cm^{-1}) were measured on a Shimadzu IRPrestige-21 FT-IR spectrophotometer. C, H, and N analyses were obtained using an Elemental Vario-EL automatic elemental analysis instrument. Mass spectrum was obtained from a Thermo Scientific Orbitrap Elite mass spectrometer. Thermogravimetric analysis (TGA) was performed on a Perkin-Elmer Pyris system. UV-vis absorption and photoluminescent spectra were recorded on a Shimadzu UV-2550 spectrometer and on a Perkin-Elmer LS-55 spectrometer, respectively. Melting points were measured by using an X-4 microscopic melting

5

point apparatus made in Beijing Taike Instrument Limited Company, and the thermometer was

uncorrected.

2.2 Synthesis and characterization of Ir(L)$_2$(acac-allyl), 7Cz-Ir(L)$_2$(acac)-POSS and 6Cz-2Ir(L)$_2$(acac)-POSS

3-allylpentane-2,4-dione (acac-allyl): Under N$_2$, a suspension of fresh sodium (3.160 g, 0.137

mol) in anhydrous toluene (60 mL) was placed in a three-necked flask. The mixture was heated up

to 120 °C and stirred vigorously till the sodium was molten and scattered, then acetylacetone

(13.750 g, 0.137 mol) was added into the mixture. The mature was stirred at 120 °C for 1 h, the

white sodium salt of β-diketone was precipitated. Allyl bromide (20 g, 0.165 mol) was added

dropwise. The reaction mixture was stirred at and refluxed overnight, then cooled and filtered to

remove excess NaBr. Toluene and the excess allyl bromide were removed by distillation, collecting

14.50 g (75.2% yield) of yellow oil at 195-196 °C. ^{1}H NMR (CDCl$_3$, 400 MHz, δ, ppm): 5.89-5.80

(m, 0.5 H), 5.75-5.66 (m, 0.5 H), 5.15-4.99 (m, 2H), 3.01-2.98 (m, 1H), 2.59 (dt, J = 7.6 Hz, J = 7.2

Hz, 2H), 2.19 (s, 3H), 2.11 (s, 3H).

9-allyl-9*H*-carbazole (Cz-allyl): A mixture of carbazole (10.0 g, 0.06 mol), potassium

hydroxide (8.98 g, 0.16 mol) and acetone (100 mL) was stirred vigorously for 2 h at room

temperature. Allyl bromide (6.6 mL, 0.072 mol) was added dropwise. After stirring for 20 h at room

temperature, the reaction mixture was poured into cold water (300 mL). The mixture was extracted

with CH$_2$Cl$_2$ (3 × 200 mL), and the combined organic phase was dried over anhydrous Na$_2$SO4.

After filtering, the filtrate was evaporated to dryness under reduced pressure. The crude was purified

by chromatography on silica gel using petroleum ether as the eluent to give Cz-allyl as a white solid

(9.1 g, 73.4%). m.p.: 51-53 °C. ^{1}H NMR (400 MHz, CDCl$_3$, δ, ppm): 8.11 (d, *J* = 8.0 Hz, 2H), 7.46

(t, J = 8.8 Hz, 2H), 7.37 (d, J = 8.0 Hz, 2H), 7.25 (t, J = 8.0 Hz, 2H), 6.03 - 5.94 (m, 1H), 5.15 (d, J = 10.6 Hz, 1H), 5.05 (d, J = 18.3 Hz, 1H), 4.91 (d, J = 4.8 Hz, 2H). Anal. Calcd for $C_{15}H_{13}N$: C, 86.92; H, 6.32; N, 6.76; Found: C, 87.02; H, 6.29; N, 6.71.

Ir(L)$_2$(acac-allyl): The cyclometalated Ir(III) μ-chlorobridged dimmer ((L)$_2$Ir(μ-Cl)$_2$Ir(L)$_2$) (1 g, 0.74 mmol), acac-allyl (0.53 g, 3.78 mmol) and anhydrous K_2CO_3 (1.00 g, 7.24 mmol) were refluxed in dichloroethane under nitrogen atmosphere for 24 h. After cooling, a small quantity of water was added. The mixture was extracted with dichloromethane (100 mL × 3). The organic phase was washed with water (2 × 100 mL) and dried over anhydrous $MgSO_4$. After filtering, the filtrate was evaporated to dryness under reduced pressure. The crude was purified by chromatography on silica gel using dichloromethane/petroleum ether/ acetone (10:10:1, v/v/v) as the eluent to give yellow powdery Ir(L)$_2$(acac-allyl) in 81.5% yield (0.47 g). ^{1}H NMR(CDCl$_3$, δ, ppm): 9.14 (d, 2H, J = 8.8 Hz, Aryl-H), 8.05 (d, 2H, J = 8.0 Hz, Aryl-H), 7.92 (t, 2H, J = 8.4 Hz, Aryl-H), 7.27 (t, 2H, J = 8.4 Hz, Aryl-H), 7.19 (d, 2H, J = 8.4 Hz, Aryl-H), 7.06 (t, 2H, J = 8.0 Hz, Aryl-H), 6.63 (t, 2H, J = 8.0 Hz, Aryl-H), 6.11 (d, 2H, J = 8.0 Hz, Aryl-H), 5.79-5.68 (m, 1H, -CH=CH$_2$), 4.90 (d, 1H, J = 8.0 Hz, -CH=CH$_2$), 4.63 (d, 1H, J = 17.2 Hz, -CH=CH$_2$), 2.86 (d, 2H, J = 2.0 Hz, -CH$_2$-), 1.80 (s, 6H, -CH$_3$). IR (KBr pellet, cm^{-1}): 3077, 2977, 2925, 2865, 1694, 1599, 1564, 1464, 1358, 1264, 1169, 987, 804, 768, 657. Anal. Calc. for $C_{36}H_{27}IrN_2O_6$ (%): C, 55.73; H, 3.51; N, 3.61. Found: C, 55.81; H, 3.57; N, 3.65. MS: Calcd for $C_{36}H_{27}IrN_2O_6$, 776.15; Found, 777.15.

7Cz-Ir(L)$_2$(acac)-POSS and 6Cz-2Ir(L)$_2$(acac)-POSS: A round bottom flask (100 mL) was charged with octakis(dimethylsiloxy)silsesquioxane (1.0 g, 0.98 mmol), Ir(L)$_2$(acac-allyl) (0.76 g, 0.98 mmol) and anhydrous toluene (30 mL). The solution was degassed with argon for 5 min and then 5 drops of a solution of platinum-1,3-divinyl-1,1,3,3-tetramethyldisiloxane (Pt-dvs) (2 wt% Pt

in xylene) were added, and the reaction mixture was stirred at room temperature under positive

argon pressure for 4 h. Then Cz-allyl (2.03 g, 9.80 mmol) was introduced, and the resulting reaction

mixture was allowed to stir at 50 ^{o}C overnight. The toluene was evaporated in vacuo and the crude

product was isolated by chromatography on silica gel using dichloromethane/ethyl acetate/petroleum

ether (1:1:8, v/v/v) as the eluent to yield pure fractions of 7Cz-Ir(L)$_2$(acac)-POSS and

6Cz-2Ir(L)$_2$(acac)-POSS, which were isolated separately in 23% and 12.5% yields.

7Cz-Ir(L)$_2$(acac)-POSS: ^{1}H NMR (400 MHz, CDCl$_3$, δ, ppm): 9.21 (d, 2H, J = 8.0 Hz,

Aryl-H), 8.42 (d, 2H, J = 5.2 Hz, Aryl-H), 8.06-8.02 (m, 16H, Aryl-H), 7.91 (t, 2H, J = 8.4 Hz,

Aryl-H), 7.41-7.35 (m, 14H, Aryl-H), 7.31-7.25 (m, 16H, Aryl-H), 7.20-7.15 (m, 16H, Aryl-H), 6.64

(t, 2H, J = 8.0 Hz, Aryl-H), 5.99 (d, 2H, J = 8.4 Hz, Aryl-H), 4.16-4.06 (m, 14H,-N-CH$_2$-), 2.52 (t,

2H, J = 7.2 Hz, -CH$_2$-), 1.80-1.76 (m, 16H, -CH$_2$-), 1.57 (s, 6H, -CH$_3$), 0.90-0.83 (m, 2H, -CH$_2$-Si),

0.60-0.51 (m, 14H, -CH$_2$-Si), 0.07-(-0.05) (m, 48H). ^{13}C NMR (CDCl$_3$, δ, ppm): 186.1, 184.2, 166.0,

157.2, 150.4, 148.0, 140.3, 139.3, 138.3, 131.6, 129.0, 125.6, 124.0, 123.6, 122.7, 120.3, 118.7,

116.1, 108.6, 77.3, 77.2, 77.0, 76.7, 45.5, 29.8, 27.1, 22.3, 14.8, 1.0, -0.4. IR (KBr pellet, cm^{-1}):

3082, 2962, 2915, 2864, 1696, 1598, 1564, 1466, 1356, 1260, 1168, 1098, 980, 802, 762, 555. MS:

Calcd for C$_{157}$H$_{174}$IrN$_9$O$_{26}$Si$_{16}$, 3244.69; Found, 3245.72.

6Cz-2Ir(L)$_2$(acac)-POSS: ^{1}H NMR (400 MHz, CDCl$_3$, δ, ppm): 9.21 (d, 2H, J = 8.4 Hz,

Aryl-H), 9.10 (d, 2H, J = 8.0 Hz, Aryl-H), 8.43 (d, 4H, J = 5.6 Hz, Aryl-H), 8.07-8.02 (m, 16H,

Aryl-H), 7.97 (t, 2H, J = 8.4 Hz, Aryl-H), 7.79 (t, 2H, J = 7.2 Hz, Aryl-H), 7.41-7.33 (m, 12H,

Aryl-H), 7.31-7.23 (m, 16H, Aryl-H), 7.20-7.13 (m, 16H, Aryl-H), 6.66-6.57 (m, 4H, Aryl-H), 6.02

(dd, 4H, J = 8.0 Hz, Aryl-H), 4.16-4.06 (m, 12H,-N-CH$_2$-), 2.59-2.49 (m, 4H, -CH$_2$-), 1.83-1.76 (m,

16H, -CH$_2$-), 1.72-1.62 (m, 12H, -CH$_3$), 0.90-0.83 (m, 4H, -CH$_2$-Si), 0.60-0.51 (m, 12H, -CH$_2$-Si),

0.07-(-0.04) (m, 48H). ^{13}C NMR (CDCl$_3$, δ, ppm): 186.0, 184.6, 166.0, 157.0, 150.7, 149.2, 147.9, 140.2, 139.3, 138.3, 131.7, 131.0, 130.5, 129.1, 125.6, 124.1, 123.5, 122.7, 120.3, 118.7, 116.3, 116.1, 108.5, 77.3, 77.0, 76.7, 45.6, 29.7, 27.2, 22.4, 14.8, 1.0, -0.4. IR (KBr pellet, cm^{-1}): 3053, 2963, 2924, 2872, 1694, 1609, 1564, 1480, 1467, 1350, 1331, 1260, 1234, 1163, 1098, 981, 839, 800, 755, 729, 554. MS: Calcd for C$_{178}$H$_{188}$Ir$_2$N$_{10}$O$_{32}$Si$_{16}$, 3813.25; Found, 3814.61.

2.3 OLEDs fabrication and characterization

The multilayer OLEDs with a device architecture of ITO/PEDOT:PSS (45 nm)/CBP: POSS materials (50 nm)/TPBi (50 nm)/Liq (2 nm)/Al(150 nm) were fabricated. Poly(3,4-ethylenedioxythiophene) doped with poly(styrenesulfonate) (PEDOT:PSS) was spin-coated onto precleaned and O$_2$-plasma-treated indium tin oxide (ITO) substrates, yielding layers ca. 45 nm thick. PEDOT:PSS layers were heated at 180 ^{o}C for 10 min to remove residual water. Blends of POSS materials + 4,4′-Bis(9-carbazolyl)biphenyl (CBP) in chlorobenzene solution was spin-coated on top of the PEDOT:PSS layers, yielding films ca. 50 nm thick. The samples were then dried at 80 ^{o}C for 30 min. A TPBi hole/exciton-blocking layer was deposited via thermal evaporation at a rate of ~ 2 Å s^{-1}. A cathode consisting of an ultrathin Liq interfacial layer with a nominal thickness of 2 nm and an Al layer ca. 150 nm thick was deposited by thermal evaporation. The deposition rates for Liq and Al were ~ 1 and 10 Å s^{-1}, respectively. The active area of the devices was 12 mm^2. The EL spectra and Commission Internationale de L'Eclairage (CIE) coordinates were measured on a Hitachi MPF-4 fluorescence spectrometer. The characterization of brightness-current-voltage (B–I–V) were measured with a 3645 DC power supply combined with a 1980A spot photometer and were recorded simultaneously. All measurements were done in the air at room temperature without any encapsulation.

9

3. Results and discussion

3.1 Synthesis and characterization of the POSS materials

The synthesis of the phosphorescent Ir(III) complex [Ir(L)$_2$(acac-allyl)] from Scheme 1 began first with preparing the ancillary ligand, 3-allylpentane-2,4-dione (acac-allyl), which has a allyl group at 3-position of pentane-2,4-dione for later attachment to POSS core. The ancillary ligand acac-allyl was successfully synthesized by reacting acetylacetone with allyl bromide in the presence of metal sodium as a base. This method leads to higher yield of the target product (75.2%). The ancillary ligand was then reacted with the chlorobridged dimer complex based on the cyclometalated coumarin ligand (3-(pyridine-2-yl)coumarin) and anhydrous K$_2$CO$_3$ in refluxing dichloroethane under nitrogen atmosphere to obtain the allyl-functionalized Ir(III) complex. Furthermore, the carbazole moiety is chosen because it has good hole-transporting properties, which was also modified with a terminal allyl for attachment to POSS core.

The hole-transporting and Ir(III) complex unit functionalized POSS materials (7Cz-Ir(L)$_2$(acac)-POSS and 6Cz-2Ir(L)$_2$(acac)-POSS) were obtained via hydrosilylation reaction in the presence of platinum(0)-1,3-divinyl-1,1,3,3-tetramethyldisiloxane (Pt-dvs) as the catalyst. The POSS materials were synthesized in a stepwise mode by sequentially reacting the Ir(III) complex Ir(L)$_2$(acac-allyl) with octakis(dimethylsiloxy)silsesquioxane (Q$_8$M$_8^H$) in a 1:1 ratio, and followed by reaction with excess Cz-allyl. 7Cz-Ir(L)$_2$(acac)-POSS and 6Cz-2Ir(L)$_2$(acac)-POSS can then be isolated from the reaction mixture chromatographically. These POSS materials were found to be completely soluble in common organic solvents (toluene, chlorobenzene, THF, chloroform, dichloromethane and acetone), and homogeneous thin films of these POSS materials were fabricated

easily by spin-coating onto the quartz glasses and indium tin oxide (ITO) substrates.

7Cz-Ir(L)$_2$(acac)-POSS and 6Cz-2Ir(L)$_2$(acac)-POSS were characterized using ^{1}H NMR, ^{13}C NMR, MS, FT-IR and X-ray diffraction (XRD) analysis. The resonance of Si-H protons in Q$_8$M$_8$[H] is located at 4.7 ppm. For Cz-allyl, two doublets (with fine coupling) and the quartet resonance proton resonance peaks from the allyl group are located at 5.03, 5.15 and 5.99 ppm with a relative molar ratio of 1:1:1, corresponding to iso-, *trans*- and substituted vinyl protons. The resonance of methylene (-CH$_2$-Cz) is observed at 4.90 ppm. The peaks from the allyl group of Ir(L)$_2$(acac-allyl) are observed at ca. 5.74, 4.90 and 4.63 ppm with a relative molar ratio of 1:1:1, corresponding to iso-, *trans*- and substituted vinyl protons. In ^{1}H NMR spectra of 7Cz-Ir(L)$_2$(acac)-POSS and 6Cz-2Ir(L)$_2$(acac)-POSS, the peaks for the vinyl groups of Cz-allyl (5.03, 5.15 and 5.99 ppm) and Ir(L)$_2$(acac-allyl) (4.63, 4.90 and ca. 5.74 ppm) and Si-H protons (4.7 ppm) disappeared, supporting the complete hydrosilylation reaction and the vinyl groups of Cz-allyl and Ir(L)$_2$(acac-allyl) underwent hydrosilylation of the Si-H bonds of Q$_8$M$_8$[H].

The FT-IR spectra of Q$_8$M$_8$[H], Ir(L)$_2$(acac-allyl) and 7Cz-Ir(L)$_2$(acac)-POSS are shown in Fig. 1. The strong absorption peak around 1098 cm^{-1} for Q$_8$M$_8$[H] and 7Cz-Ir(L)$_2$(acac)-POSS represented the vibrations of the siloxane Si-O-Si groups, and it is a general feature of POSS derivatives. The characteristic stretching vibration of the Si-H groups of Q$_8$M$_8$[H] appears as a signal at 2147 cm^{-1}. In 7Cz-Ir(L)$_2$(acac)-POSS, the peak for the Si-H groups disappeared completely, indicating that the hydrosilylation occurred to completion. The characteristic stretching vibration bands of -CH$_3$ and -CH$_2$- are clearly observed at 2800 – 2900 cm^{-1}. The FT-IR spectrum of 6Cz-2Ir(L)$_2$(acac)-POSS was similar to that of 7Cz-Ir(L)$_2$(acac)-POSS.

Fig. 2 presents the X-ray diffraction (XRD) patterns of Cz-allyl, Ir(L)$_2$(acac-allyl),

11

7Cz-Ir(L)$_2$(acac)-POSS and 6Cz-2Ir(L)$_2$(acac)-POSS. Cz-allyl and Ir(L)$_2$(acac-allyl) exhibit several

sharp XRD peaks because of their crystallinity, suggesting that Cz-allyl and Ir(L)$_2$(acac-allyl) show

the crystal morphology. Interestingly, the attachment of Cz-allyl and Ir(L)$_2$(acac-allyl) to the POSS

core led to the disappearance of these sharp peaks except for a sharp peak at 5.9^{o}, which were

replaced by a broad amorphous halo appearing at ca. 21°, indicating that the crystalline Cz-allyl and

Ir(L)$_2$(acac-allyl) became amorphous state after their attachments to the POSS cage.

The thermogravimetric analyses (TGA) were performed in flowing drying nitrogen atmosphere

at the heating rate of 10 ^{o}C/min. In a comparison of the thermal stabilities, we used the complex

Ir(L)$_2$(acac-allyl) as the contrastive sample. The result of TGA measurements of Ir(L)$_2$(acac-allyl)

and the POSS materials are shown in Fig. 3. An increase in the decomposition temperature of the

POSS materials compared with Ir(L)$_2$(acac-allyl) was observed. At about 352 and 379 ^{o}C, there are

two sharp weight losses in the TGA cueve of Ir(L)$_2$(acac-allyl), it shows that the complex

Ir(L)$_2$(acac-allyl) undergoes two large-stage decomposition processes. For the POSS materials, at

373 ^{o}C the materials began to decompose, and corresponding to a sharp weight loss in their TGA

curves. Compared with Ir(L)$_2$(acac-allyl), the inorganic silsesquioxane (POSS) provided additional

heat capacity, thereby stabilizing the materials against thermal decomposition.

3.2 Electrochemical, optical and electroluminescence properties of the POSS materials

The UV-vis absorption and photoluminescence spectra of Ir(L)$_2$(acac-allyl),

7Cz-Ir(L)$_2$(acac)-POSS and 6Cz-2Ir(L)$_2$(acac)-POSS were measured in diluted dichloromethane

solutions, as shown in Fig. 4. The absorption spectrum of the complex Ir(L)$_2$(acac-allyl) exhibits two

intense absorption bands at about 227 and 274 nm, and three weak absorption bands at 345, 384 and

438 nm, respectively, in which the absorption bands below 360 nm could be ascribed to

spin-allowed π-π* transitions of the ligands, the band around 384 nm can be assigned to the spin-allowed metal-to-ligand charge transfer [1]MLCT (metal-ligand-charge-transfer), and the band at the longer wavelength (438 nm) can be assigned to both spin-orbit coupling enhanced $^3(\pi \rightarrow \pi^*)$ and spin-forbidden [3]MLCT transitions [30-32].

The absorption spectra of 7Cz-Ir(L)$_2$(acac)-POSS and 6Cz-2Ir(L)$_2$(acac)-POSS approximately resemble each other, which can be described as two components: an intense absorption region in high energy region ranging from 220 to 360 nm and a weak absorption region in low energy region ranging from 360 to 480 nm. In intense absorption region, there are five visible absorption peaks at 236 (246), 262, 295, 335 and 346 nm, which can be attributed to the $\pi \rightarrow \pi^*$ transitions of the ligands. In weak absorption region, there are two absorption peaks at 384 and 440 nm, the former can be assigned to the spin-allowed metal-to-ligand charge transfer [1]MLCT, the latter can be assigned to both spin-orbit coupling enhanced $^3(\pi \rightarrow \pi^*)$ and spin-forbidden [3]MLCT transitions.

The photoluminescence spectra of Ir(L)$_2$(acac-allyl), 7Cz-Ir(L)$_2$(acac)-POSS and 6Cz-2Ir(L)$_2$(acac)-POSS strongly resemble each other, they all exhibit a strong green emission with a maximum main peak at 530 nm and a shoulder peak at 567 nm.

The quantum yields of Ir(L)$_2$(acac-allyl), 7Cz-Ir(L)$_2$(acac)-POSS and 6Cz-2Ir(L)$_2$(acac)-POSS at room temperature were measured to be 9.15%, 9.43% and 9.39% from the THF solutions (ca. 10^{-6} mol/L) by an absolute method using the Edinburgh Instruments (FLS920) integrating sphere excited at 380 nm with the Xe lamp. The lifetime decays of Ir(L)$_2$(acac-allyl), 7Cz-Ir(L)$_2$(acac)-POSS and 6Cz-2Ir(L)$_2$(acac)-POSS were measured to be ($\tau_1 = 0.79$ μs, $\tau_2 = 9.22$ μs), ($\tau_1 = 0.89$ μs, $\tau_2 = 9.27$ μs) and ($\tau_1 = 1.41$ μs, $\tau_2 = 9.85$ μs) by a time-correlated single photon counting spectrometer using Edinburgh Instruments (FLS920) with a microsecond flashlamp as the excitation source (repetition

rate 90 Hz) at room temperature (Supplementary Fig. S1-S3).

Cyclic voltammetry (CV) was employed to investigate the electrochemical behavior of the POSS materials. The highest occupied molecular orbital (HOMO) and the lowest unoccupied molecular orbital (LUMO) energy levels of the POSS materials were calculated from their cyclic voltammetry measurements and their absorption spectra. The POSS materials were dissolved in dichloromethane with tetra-*n*-butylammonium tetrafluoroborate (0.1 mol/L) as the electrolyte. A platinum working electrode and a saturated Ag/AgCl reference electrode were used. Ferrocene was used for potential calibration. As shown in Fig. 5, the potentials for oxidation of the POSS materials were observed to be 0.88 and 0.89 V, respectively. At the same condition, the oxidation peak and the reductive peak of ferrocene were observed at 0.56 and 0.32 V, respectively, then the $E_{1/2}$ (Fc/Fc$^+$) is 0.44 V. Thus the HOMO energy levels of 7Cz-Ir(L)$_2$(acac)-POSS and 6Cz-2Ir(L)$_2$(acac)-POSS were determined to be -5.24 and -5.25 eV regarding the energy level of ferrocene/ferrocenium as -4.80 eV [33]. The optical band edge of the POSS materials was estimated to be 468 nm, which corresponds to 2.65 eV. Then the LUMO energy levels of the POSS materials are calculated to be -2.59 and -2.60 eV, respectively. The cyclic voltammetry curve of Ir(L)$_2$(acac-allyl) was also shown in Fig. 5. From its oxidation potential (1.11 V) and optical band edge (471 nm), the HOMO and LUMO energy levels of Ir(L)$_2$(acac-allyl) are calculated to be -5.47 and -2.84 eV, which are lower in contrast with the HOMO and LUMO energy levels of the POSS materials.

Table 1 summarizes the photophysical, thermal and electrochemical properties of the POSS materials. While attachment of Ir(III) complex on the POSS core has no significant effects on the photophysical properties of the materials, it does significantly increase the thermal stability compared with the parent Ir(III) complex.

To investigate the electroluminescence (EL) properties of the POSS materials, the light-emitting devices with the architecture of ITO/PEDOT:PSS (45 nm)/CBP: POSS materials (50 nm)/TPBi (50 nm)/Liq (2 nm)/Al(150 nm) have been made and fabricated. The emitting layers are consisted of host materials CBP and dopants of the POSS materials at different concentrations (x wt%), and prepared by solution-processable method. TPBi was used as the electron transport and hole/exciton-blocking material. Liq was used as the electron-injection layer. CBP and the POSS materials were dissolved in 1,2-dichlorobenzene, and their concentrations were prepared to be 20 mg/mL. The mixture solutions with different volume ratios between CBP and the POSS materials were used to fabricate the emitting layers (spin speed: 1000 rpm/min).

The electroluminescence (EL) spectra of the devices based on 7Cz-Ir(L)$_2$(acac)-POSS and 6Cz-2Ir(L)$_2$(acac)-POSS with different dopant concentrations and at different voltages are shown in Fig. 6 and 7. Exclusive emissions from the Ir(III) complex were found in the EL spectra of the devices, which were independent of the different dopant concentrations and at different driving voltages. The doped devices of the POSS materials exhibit green emissions with a maximum main peak at 530 nm and a shoulder peak at 567 nm, it was indicated that the EL spectra of the POSS materials resemble closely their PL spectra in dichloromethane solutions. The Commission Internationale de L′Eclairage (CIE) coordinates of the devices based on 7Cz-Ir(L)$_2$(acac)-POSS and 6Cz-2Ir(L)$_2$(acac)-POSS are (0.39, 0.61) and (0.41, 0.60), respectively.

The luminance *vs.* the driving voltage and the current efficiency *vs.* the driving voltage characteristics of the devices fabricated with different 7Cz-Ir(L)$_2$(acac)-POSS doping concentrations are shown in Fig. 8 and 9. Table 2 summarized the performances of the devices based on the POSS materials. As shown in Fig. 8, at doped concentration ratios between CBP and

15

7Cz-Ir(L)$_2$(acac)-POSS were 1:2, 1:1, 2:1, 3:1, 4:1, 6:1 and 8:1, the turn-on voltages (V$_{on}$) of the devices (to achieve the luminance of 1 cd/m^2) are between 6.3 V and 6.7 V. The difference of the turn-on voltages is not large, but at the same luminance (for example, 5000 cd/m^2) the luminance *vs.* the driving voltage characteristics of the devices shift to higher drive voltages, where the driving voltages are 11.19, 11.11, 12.50, 13.70, 15.52, 15.72 and 15.37 V. At a driving voltage of 15.6 V, brightness of 18360, 19530, 14019, 11735, 5185, 4236 and 6392 cd/cm^2 were observed in the devices with 1:2, 1:1, 2:1, 3:1, 4:1, 6:1 and 8:1 between CBP and 7Cz-Ir(L)$_2$(acac)-POSS, respectively. The devices based on 7Cz-Ir(L)$_2$(acac)-POSS with 3:1 doping concentration showed a maximum luminance of 21285 cd/m^2 at 19.3 V. Fig. 9 shows the relationship between luminous efficiency and the driving voltage in the devices fabricated with different 7Cz-Ir(L)$_2$(acac)-POSS doping concentrations. It was found that the luminous efficiency showed a downward trend with decreasing the weight ratio of 7Cz-Ir(L)$_2$(acac)-POSS. When the doping concentration is 1:1 between CBP and 7Cz-Ir(L)$_2$(acac)-POSS, a maximum luminous efficiency of 28.22 cd/A at 8.9 V and a maximum external quantum efficiency (EQE) of 7.82% were achieved in the devices based on 7Cz-Ir(L)$_2$(acac)-POSS. By comparison of the performances of different doping concentrations, we can see that the doped devices exhibited higher luminous efficiency at lower CBP concentrations, it can be attributed to improved balance of carrier injection and transport.

Fig. 10 and 11 display the luminance *vs.* the driving voltage and the current efficiency *vs.* the driving voltage characteristics of the devices based on 6Cz-2Ir(L)$_2$(acac)-POSS at different doping concentrations 1:2, 1:1, 2:1 and 3:1 between CBP and 6Cz-2Ir(L)$_2$(acac)-POSS. The performances of the devices with various 6Cz-2Ir(L)$_2$(acac)-POSS doping concentrations in CBP host are summarized in Table 2. The device with 2:1 doping concentration exhibited the best EL performance.

The device had a maximum brightness of 18300 cd/m^2 at 15.6 V and a maximum current efficiency of 25.12 cd/A at 8.9 V and a maximum external quantum efficiency (EQE) of 6.96%.

As can be observed from the Table 2, the electroluminescent performance of the devices based on 7Cz-Ir(L)$_2$(acac)-POSS is substantially higher than that of the devices based on 6Cz-2Ir(L)$_2$(acac)-POSS, indicating that concentration quenching leads to the reduction in device efficiency with increasing amounts of the Ir(III) complex units on the POSS core. The device efficiency and brightness increase as the Ir(III) complex unit content on the POSS materials decreases, which can be attributed to reduced interactions among the Ir(III) complex units and diminished concentration quenching. Similar phenomenon was reported by Yang and co-workers [34]. As shown in Table 2, the turn-on voltages for the OLEDs are relatively high. Probably, it caused by mismatching the energy levels of the different layers.

4. Conclusions

We have reported on the synthesis, photophysical and electrochemical characterization, and thermal stabilities of two inorganic/organic hybrid materials, 7Cz-Ir(L)$_2$(acac)-POSS and 6Cz-2Ir(L)$_2$(acac)-POSS, consisting of an emissive Ir(III) complex and carbazole moieties covalently attached to a polyhedral oligomeric silsesquioxane (POSS) core. Compared with the emissive Ir(III) complex (Ir(L)$_2$(acac-allyl)), the inorganic/organic hybrid materials have good thermal stability due to the inorganic POSS core. Attachment of Ir(III) complex on the POSS core has no significant effects on the photophysical properties of the POSS materials. Solution processed light-emitting devices based on the POSS materials exhibited ultrahigh brightness and higher external quantum efficiency. At the doping concentration of 3:1 between CBP and

7Cz-Ir(L)$_2$(acac)-POSS, the devices based on 7Cz-Ir(L)$_2$(acac)-POSS exhibited green emission with a maximum luminance of 21285 cd/m^2 at 19.3 V. When the doping concentration is 1:1 between CBP and 7Cz-Ir(L)$_2$(acac)-POSS, a maximum luminous efficiency of 28.22 cd/A at 8.9 V and a maximum external quantum efficiency (EQE) of 7.82% were achieved in the devices based on 7Cz-Ir(L)$_2$(acac)-POSS. For 6Cz-2Ir(L)$_2$(acac)-POSS, at the doping concentration of 2:1 between CBP and 6Cz-2Ir(L)$_2$(acac)-POSS, the device had a maximum brightness of 18300 cd/m^2 at 15.6 V and a maximum current efficiency of 25.12 cd/A at 8.9 V and a maximum external quantum efficiency (EQE) of 6.96%. Furthermore, the device efficiency and brightness increase as the Ir(III) complex unit content on the POSS materials decreases, which can be attributed to reduced interactions among the Ir(III) complex units and diminished concentration quenching.

Supplementary material:

Fig. S1-S3 are given as supplementary information.

Acknowledgements

18

References

[1] M. A. Baldo, D. F. O′Brian, Y, You, A. Shoustikov, S. Sibley, M. E. Thompson, S. R. Forrest, Highly efficient phosphorescent emission from organic electroluminescent devices, Nature 1998, 395, 151-154.

[2] M. Thompson, The evolution of organometallic complexes in organic light-emitting devices, MRS Bulletin 2007, 32, 694-701.

[3] W.-Y. Wong, C.-L. Ho, Heavy metal organometallic electrophosphors derived from multi-component chromophores, Coord. Chem. Rev. 2009, 253, 1709-1758.

[4] Y. Chi, P.-T. Chou, Transition-metal phosphors with cyclometalating ligands: fundamentals and applications, Chem. Soc. Rev. 2010, 39, 638-655.

[5] Y. You, S. Y. Park, Phosphorescent iridium(iii) complexes: toward high phosphorescence quantum efficiency through ligand control, Dalton Trans. 2009, 1267-1282.

[6] L. X. Xiao, Z. J. Chen, B. Qu, J. X. Luo, S. Kong, Q. H. Gong, J. Kido, Recent Progresses on Materials for Electrophosphorescent Organic Light-Emitting Devices, Adv. Mater. 2011, **23**, 926-952.

[7] R. D. Costa, E. Ortí, H. J. Bolink, S. Graber, C. E. Housecroft, E. C. Constable, Efficient and long-living light-emitting electrochemical cells, Adv. Funct. Mater. 2010, 20, 1511-1520.

[8] M. X. Yu, Q. Zhao, L. X. Shi, F. Y. Li, Z. G. Zhou, H. Yang, T. Yia, C. H. Huang, Cationic iridium(III) complexes for phosphorescence staining in the cytoplasm of living cells, Chem. Commun. 2008, 2115-2117.

[9] D.-L. Ma, H.-Z. He, D. S.-H. Chan, C.-Y. Wong, C.-H. Leung, A colorimetric and luminescent dual-modal assay for Cu(II) ion detection using an iridium(III) complex, PLOS ONE, 2014, 9,

e99930.

[10] K. K.-W. Lo, W.-K. Hui, C.-K. Chung, K. H.-K. Tsang, D.C.-M. Ng, N. Zhu, K.-K. Cheung, Biological labelling reagents and probes derived from luminescent transition metal polypyridine complexes, Coord. Chem. Rev. 2005, 249, 1434-1450.

[11] E. Orselli, G. S. Kottas, A. E. Konradsson, P. Coppo, R. Fröhlich, L. D. Cola, A. van Dijken, M. Büchel, H. Börner, Blue-emitting iridium complexes with substituted 1,2,4-triazole ligands: Synthesis, photophysics, and devices, Inorg. Chem. 2007, 46, 11082-11093.

[12] G. J. Zhou, W.-Y. Wong, B. Yao, Z. Y. Xie, L. X. Wang, Triphenylamine-dendronized pure red iridium phosphors with superior OLED efficiency/color purity trade-offs, Angew. Chem. Int. Ed. 2007, 46, 1149-1151.

[13] C. Rothe, C.-J. Chiang, V. Jankus, K. Abdullah, X. Zeng, R. Jitchati, A. S. Batsanov, M. R. Bryce, A. P. Monkman, Ionic iridium(III) complexes with bulky side groups for use in light emitting cells: Reduction of concentration quenching, Adv. Funct. Mater. 2009, 19, 2038-2044.

[14] X. S. Zeng, M. Tavasli, I. F. Perepichka, A. S. Batsanov, M. R. Bryce, C.-J. Chiang, C. Rothe, A. P. Monkman, Cationic bis-cyclometallated iridium(III) phenanthroline complexes with pendant fluorenyl substituents: Synthesis, redox, photophysical properties and light-emitting cells, Chem.–Eur. J. 2008, 14, 933-943.

[15] C. Hartmann-Thompson (Ed.); "Applications of Polyhedral Oligomeric Silsesquioxanes" - Advances in Silicon Science, Vol. 3, 2011.

[16] R. M. Laine, Nanobuilding blocks based on the $[OSiO_{1.5}]_x$ (x = 6, 8, 10) octasilsesquioxanes, J. Mater. Chem. 2005, 15, 3725-3744.

[17] D. B. Cordes, P. D. Lickiss, F. Rataboul, Recent developments in the chemistry of cubic

polyhedral oligosilsesquioxanes, Chem. Rev. 2010, 110, 2081-2173.

[18] K. Tanaka, Y. Chujo, Advanced functional materials based on polyhedral oligomeric silsesquioxane (POSS), J. Mater. Chem. 2012, 22, 1733-1746.

[19] F. K. Wang, X. H. Lu, C. B. He, Some recent developments of polyhedral oligomeric silsesquioxane (POSS)-based polymeric materials, J. Mater. Chem. 2011, 21, 2775-2782.

[20] (a) K. L. Chan, P. Sonar, A. Sellinger, Cubic silsesquioxanes for use in solution processable organic light emitting diodes (OLED), J. Mater. Chem., 2009, 19, 9103-9120; (b) D. M. Sun, Z. J. Ren, M. R. Bryce, S. K. Yan, Arylsilanes and siloxanes as optoelectronic materials for organic light-emitting diodes (OLEDs), J. Mater. Chem. C, 2015, DOI:10.1039/c5tc01638j.

[21] (a) X. H. Yang, J. D. Froehlich, H.S. Chae, S. Li, A. Mochizuki, G.E. Jabbour, Efficient Light-Emitting Devices Based on Phosphorescent Polyhedral Oligomeric Silsesquioxane Materials, Adv. Funct. Mater., 2009, 19, 2623–2629; (b) Z. J. Ren, R. B. Zhang, Y. G. Ma, F. Wang, S. K. Yan, Synthesis of ring-structured polysiloxane as host materials for blue phosphorescent device, J. Mater. Chem., 2011, 21, 7777-7781; (c) Z. J. Ren, Z. Z. Chen, W. X. Fu, R. B. Zhang, F. Z. Shen, F. Wang, Y. G. Ma, S. K. Yan, Ladder polysilsesquioxane for wide-band semiconductors: synthesis, optical properties and doped electrophosphorescent device, J. Mater. Chem., 2011, 21, 11306–11311; (d) D. M. Sun, Q. Fu, Z. J. Ren,W. Li, H. H. Li, D. G. M, S. K. Yan, Carbazole-based polysiloxane hosts for highly efficient solution-processed blue electrophosphorescent devices, J. Mater. Chem. C, 2013, 1, 5344–5350.

[22] A. Sellinger, R.M. Laine, Organic-inorganic hybrid light emitting devices (HLED), US Pat. 6517958, 2003.

[23] S. Xiao, M. Nguyen, X. Gong, Y. Cao, H.B. Wu, D. Moses, A.J. Heeger, Stabilization of

semiconducting polymers with silsesquioxane, Adv. Funct. Mater., 2003, 13, 25-29.

[24] J. Lee, H. J. Cho, N. S. Cho, D. H. Hwang, H. K. Shim, Synthesis of polyhedral oligomeric silsesquioxane-functionalized polyfluorenes: Hybrid organic–inorganic π-conjugated polymers, Synth. Met., 2006, 156, 590-596.

[25] J. Lee, H. J. Cho, N. S. Cho, D. H. Hwang, J. M. Kang, E. Lim, J. I. Lee, H. K. Shim, Enhanced efficiency of polyfluorene derivatives: Organic–inorganic hybrid polymer light-emitting diodes, J. Polym. Sci. Part A: Polym. Chem., 2006, 44, 2943-2954.

[26] X. H. Yang, J. D. Froehlich, H. S. Chae, B. T. Harding, S. Li, A. Mochizuki, G. E. Jabbour, Efficient light-emitting devices based on platinum-complexes-anchored polyhedral oligomeric silsesquioxane materials, Chem. Mater., 2010, 22, 4776–4782.

[27] M. Singh, H. S. Chae, J. D. Froehlich, T. Kondou, S. Li, A. Mochizuki, G. E. Jabbour, Electroluminescence from printed stellate polyhedral oligomeric silsesquioxanes, Soft Matter., 2009, 5, 3002–3005.

[28] (a) T. Z. Yu, Y. Cao, W. M. Su, C. C. Zhang, Y. L. Zhao, D. W. Fan, M. J. Huang, K. Yue, Stephen Z. D. Cheng, Synthesis, structure, photo- and electro-luminescence of an iridium(III) complex with novel carbazole functionalized β-diketone ligand, RSC Advances, 2014, 4, 554-562; (b) T. Z. Yu, Y. L. Shi, H. F. Chai, L. X. Niu, P. Liu, Y. L. Zhao, J. D. Kang, B. Gao, H. Zhang, Synthesis, characterization, and photo- and electro-luminescence of Ir(III) complexes containing carrier transporting group-substituted β-diketonate ligand, RSC Advances, 2014, 4, 11680-11688.

[29] T. Z. Yu, S. D. Yang, Y. L. Zhao, H. Zhang, D. W. Fan, X. Q. Han, Z. M. Liu, Synthesis, crystal structure and photoluminescent property of an iridium complex with coumarin derivative ligand. Inorg Chim Acta 2011; 379: 171-174.

[30] H. H. Rho, G. Y. Park, Y. Ha, Y. S. Kim, Synthesis and Photophysical Studies of Iridium Complexes Having Different Ligands, Jpn. J. Appl. Phys., 2006, 45, 568-573.

[31] Z. Bao, A.J. Lovinger, J. Brown, New Air-Stable n-Channel Organic Thin Film Transistors, J. Am. Chem. Soc., 1998, 120, 207-208.

[32] Y. Wang, N. Herron, V. V. Grushin, D. LeCloux, V. Petrov, Highly efficient electroluminescent materials based on fluorinated organometallic iridium compounds, Appl. Phys. Lett., 2001, 79, 449-451.

[33] J. Pommerehne, H. Vestweber, W. Guss, R. F. Mahrt, H. Bässler, M. Porsch, J. Daub, Efficient two layer leds on a polymer blend basis, Adv. Mater., 1995, 7, 551-554.

[34] X. H. Yang, J. D. Froehlich, H. S. Chae, B. T. Harding, S. Li, A. Mochizuki, G.E. Jabbour, Efficient light-emitting devices based on platinum-complexes-anchored polyhedral oligomeric silsesquioxane materials, Chem. Mater., 2010, 22, 4776-4782.

Legend:

Scheme 1. The synthetic routes of 7Cz-Ir(L)$_2$(acac)-POSS and 6Cz-2Ir(L)$_2$(acac)-POSS.

Fig. 1. The FT-IR spectra of Q$_8$M$_8^H$, Ir(L)$_2$(acac-allyl) and 7Cz-Ir(L)$_2$(acac)-POSS.

Fig. 2. The X-ray diffraction (XRD) patterns of Cz-allyl, Ir(L)$_2$(acac-allyl), 7Cz-Ir(L)$_2$(acac)-POSS and 6Cz-2Ir(L)$_2$(acac)-POSS.

Fig. 3. Thermogravimetric analyses (TGA) of Ir(L)$_2$(acac-allyl), 7Cz-Ir(L)$_2$(acac)-POSS and 6Cz-2Ir(L)$_2$(acac)-POSS.

Fig. 4. UV-vis absorption and photoluminescence spectra of Ir(L)$_2$(acac-allyl), 7Cz-Ir(L)$_2$(acac)-POSS and 6Cz-2Ir(L)$_2$(acac)-POSS in diluted dichloromethane solutions. (C = 1.0 × 10^{-5} mol/L)

Fig. 5. Cyclic voltammograms of ferrocene and the POSS materials. (scan rate: 10 mV/s, solvent: dichloromethane)

Fig. 6. EL spectra of 7Cz-Ir(L)$_2$(acac)-POSS at different doped concentrations (a) and different voltages (b). Device configuration: ITO/PEDOT:PSS (45 nm)/CBP: 7Cz-Ir(L)$_2$(acac)-POSS (50 nm, v/v)/TPBi (50 nm)/Liq (2 nm)/Al(150 nm).

Fig. 7. EL spectra of 6Cz-2Ir(L)$_2$(acac)-POSS at different doped concentrations (a) and different voltages (b). Device configuration: ITO/PEDOT:PSS (45 nm)/CBP: 6Cz-2Ir(L)$_2$(acac)-POSS (50 nm, v/v)/TPBi (50 nm)/Liq (2 nm)/Al(150 nm).

Fig. 8. Luminance *vs.* voltage characteristics of the devices with different volume ratios between CBP and 7Cz-Ir(L)$_2$(acac)-POSS. Device configuration: ITO/PEDOT:PSS (45 nm)/CBP: 7Cz-Ir(L)$_2$(acac)-POSS (50 nm, v/v)/TPBi (50 nm)/Liq (2 nm)/Al(150 nm).

(Concentrations of CBP and 7Cz-Ir(L)$_2$(acac)-POSS: 20 mg/mL)

Fig. 9. Current efficiency *vs.* voltage characteristics of the devices with different volume ratios between CBP and 7Cz-Ir(L)$_2$(acac)-POSS. Device configuration: ITO/PEDOT:PSS (45 nm)/CBP: 7Cz-Ir(L)$_2$(acac)-POSS (50 nm, v/v)/TPBi (50 nm)/Liq (2 nm)/Al(150 nm). (Concentrations of CBP and 7Cz-Ir(L)$_2$(acac)-POSS: 20 mg/mL)

Fig. 10. Luminance *vs.* voltage characteristics of the devices with different volume ratios between CBP and 6Cz-2Ir(L)$_2$(acac)-POSS. Device configuration: ITO/PEDOT:PSS (45 nm)/CBP: 6Cz-2Ir(L)$_2$(acac)-POSS (50 nm, v/v)/TPBi (50 nm)/Liq (2 nm)/Al(150 nm). (Concentrations of CBP and 6Cz-2Ir(L)$_2$(acac)-POSS: 20 mg/mL)

Fig. 11. Current efficiency *vs.* voltage characteristics of the devices with different volume ratios between CBP and 6Cz-2Ir(L)$_2$(acac)-POSS. Device configuration: ITO/PEDOT:PSS (45 nm)/CBP: 6Cz-2Ir(L)$_2$(acac)-POSS (50 nm, v/v)/TPBi (50 nm)/Liq (2 nm)/Al(150 nm). (Concentrations of CBP and 6Cz-2Ir(L)$_2$(acac)-POSS: 20 mg/mL)

Table 1. Photophysical, thermal and electrochemical properties of the POSS materials.

Table 2. EL performances of the POSS materials.
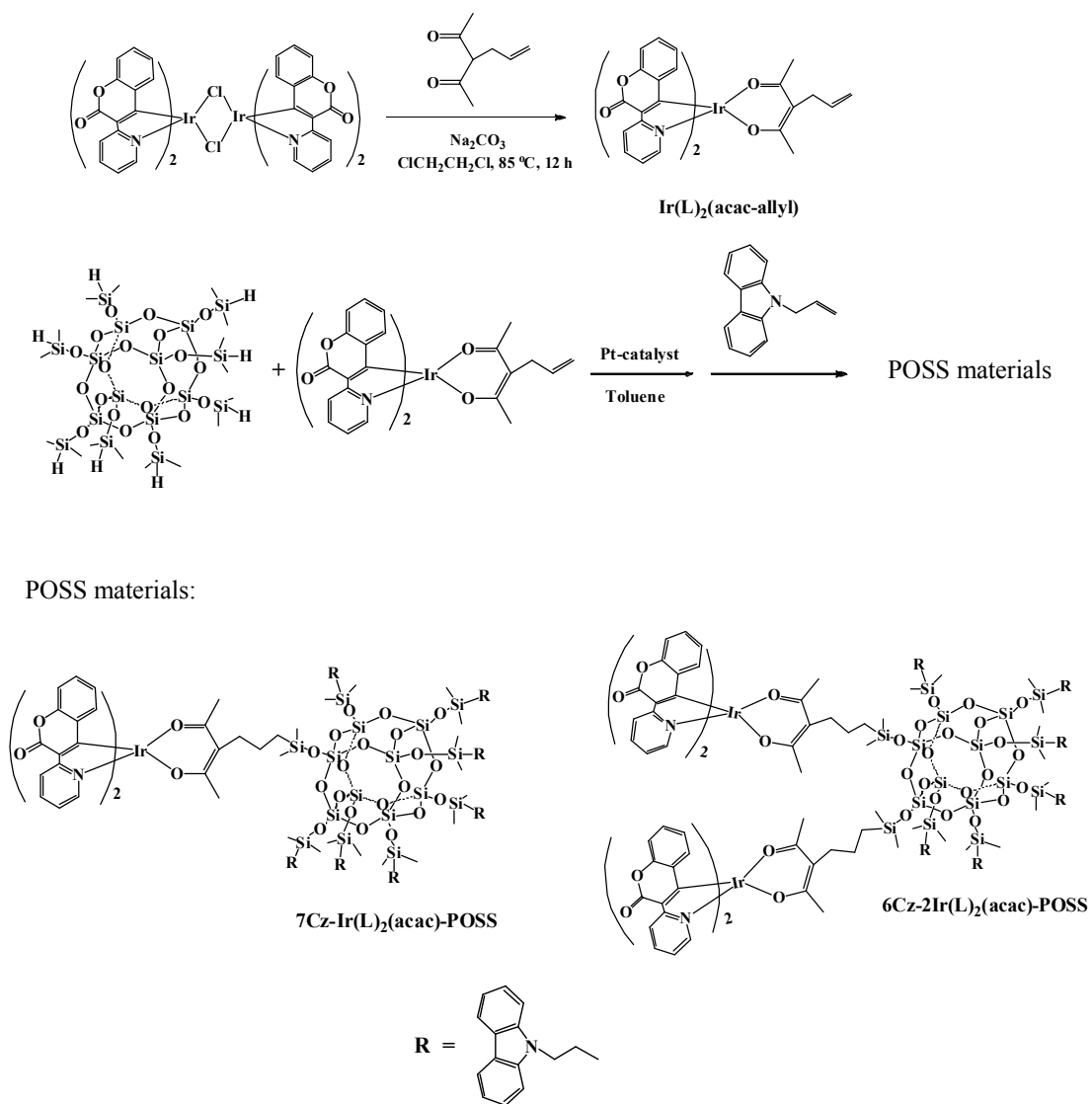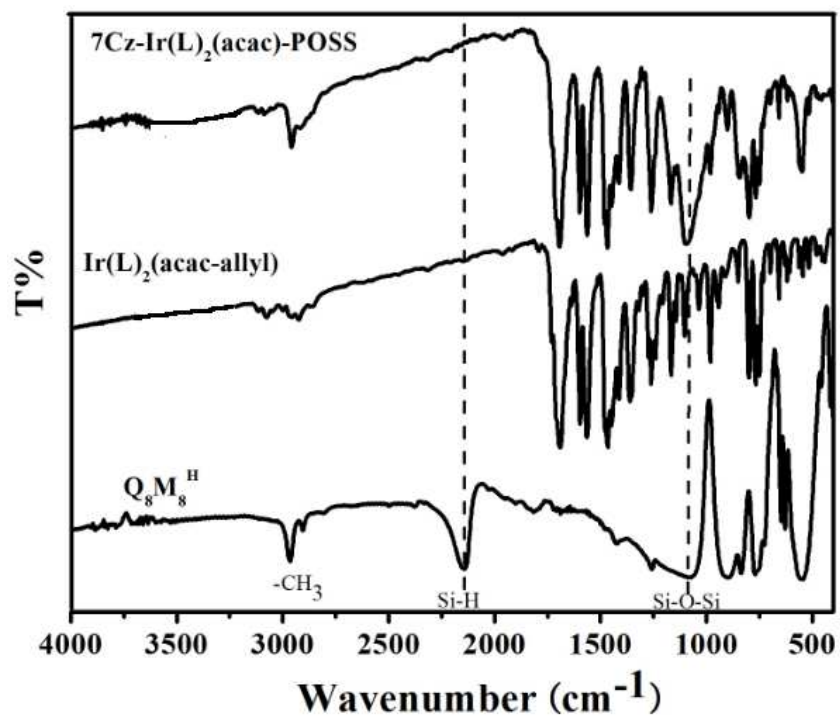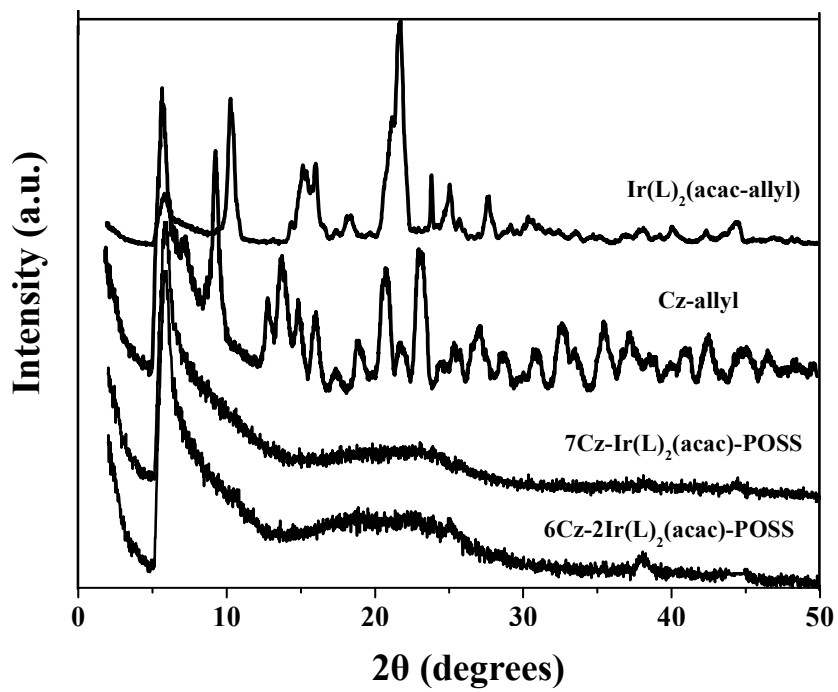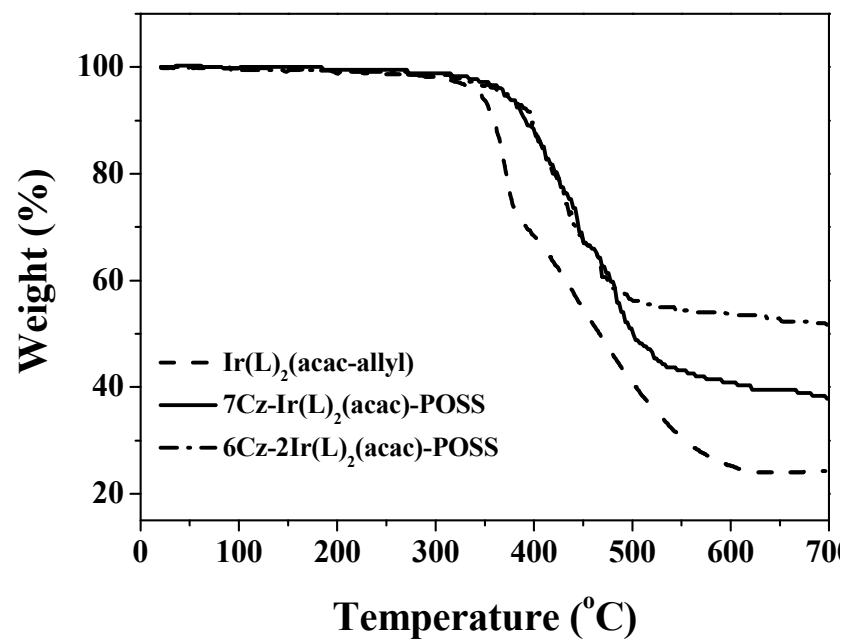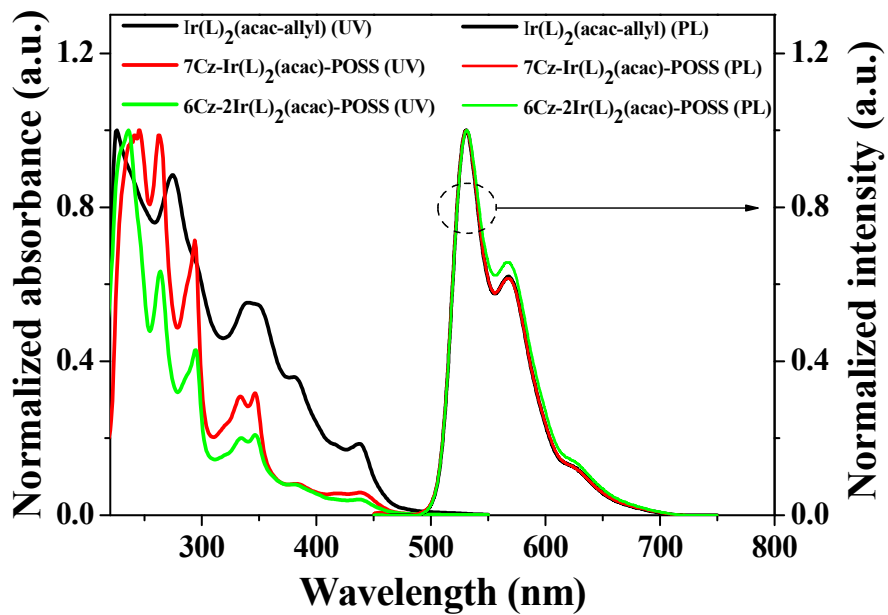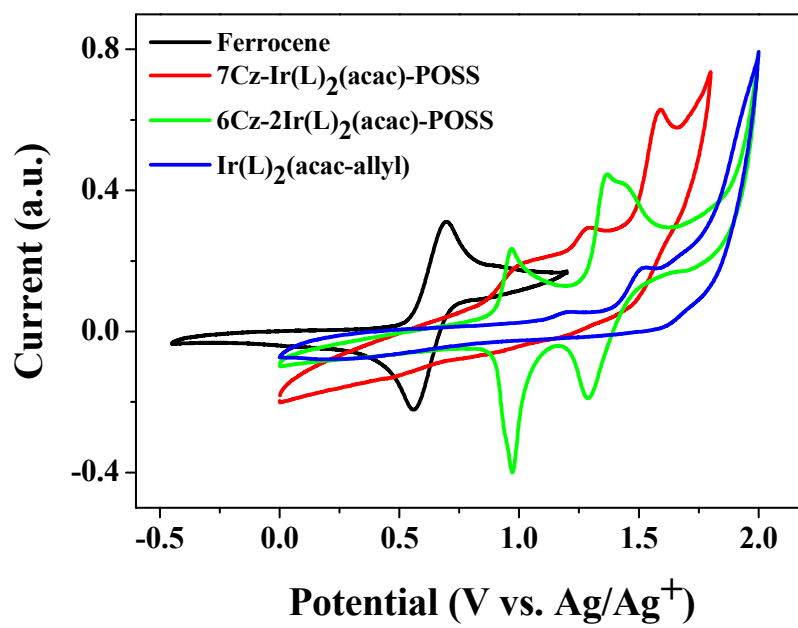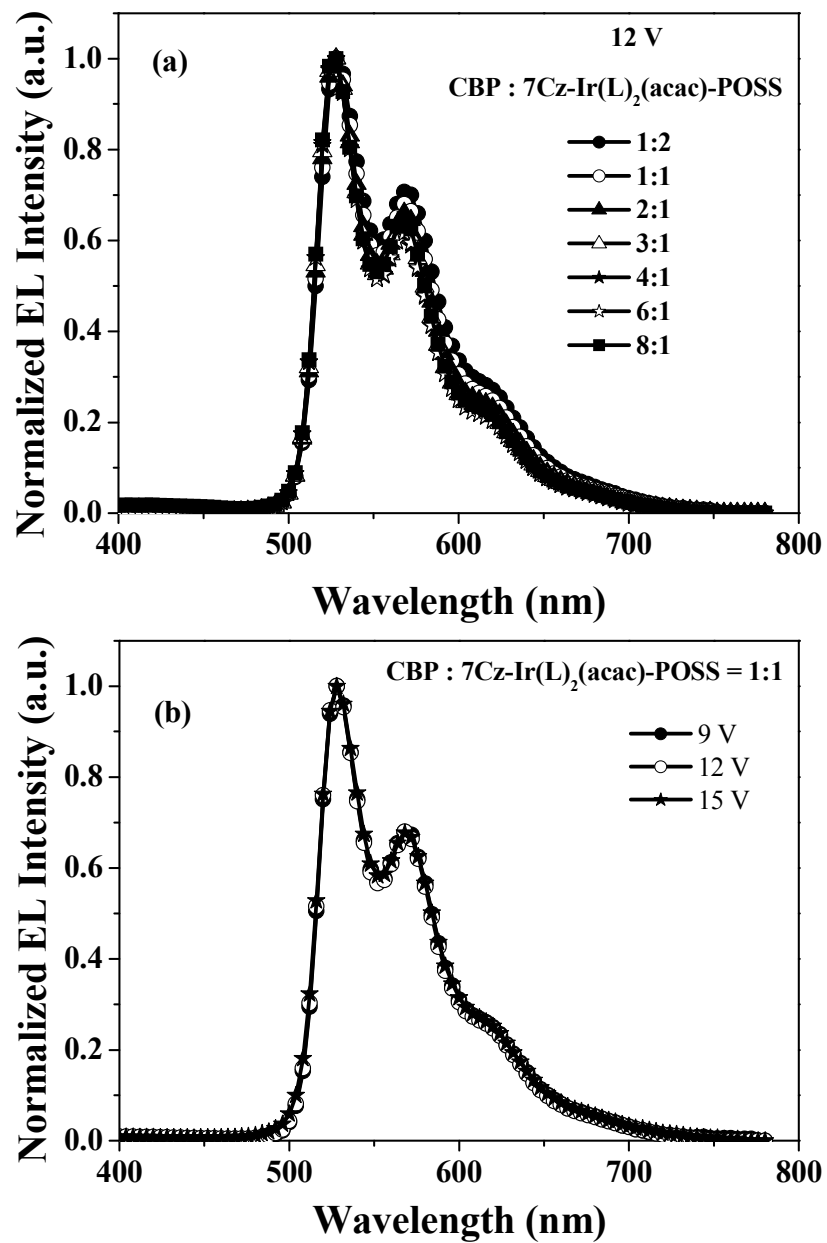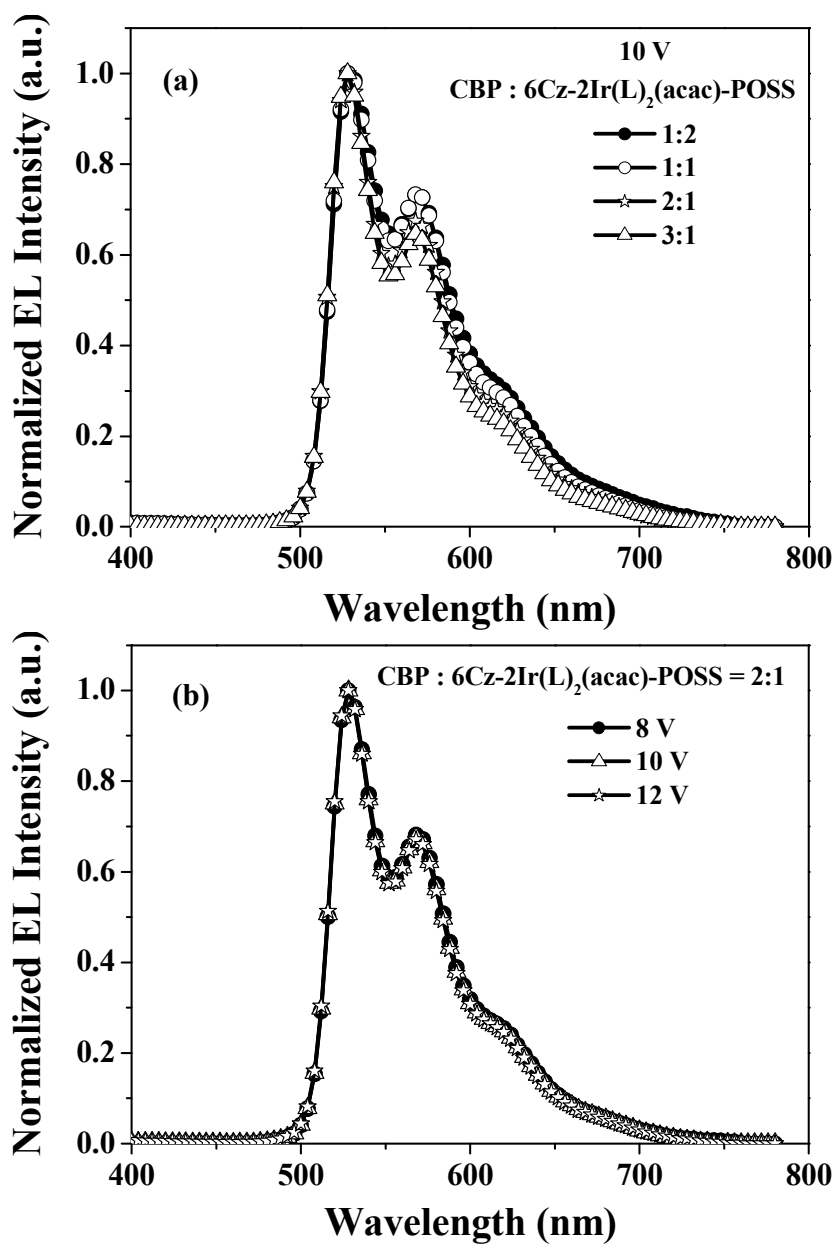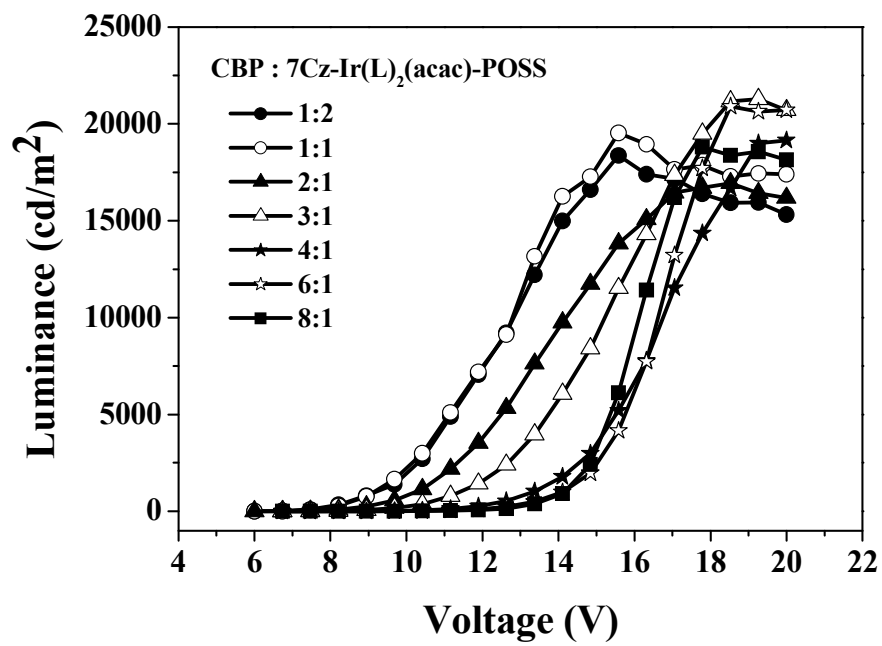
Ir(L)₂(acac-allyl)

POSS materials

POSS materials:

7Cz-Ir(L)₂(acac)-POSS

6Cz-2Ir(L)₂(acac)-POSS

R =

Scheme 1.

Fig. 1

27

Fig. 2

28

Fig. 3

29

Fig. 4

30

Fig. 5

31

Fig. 6

32

Fig. 7

33

Fig. 8

34

Fig. 9

35

Fig. 10

Fig. 11

37
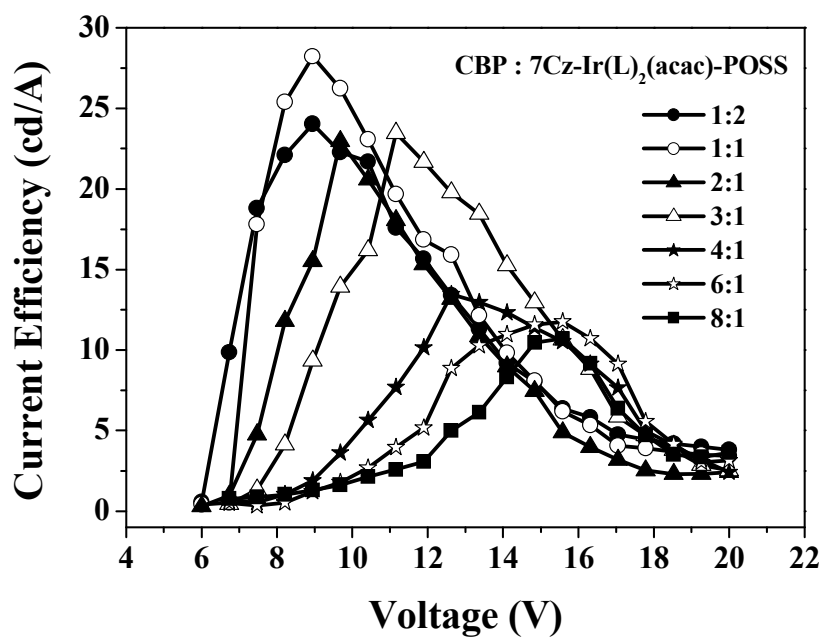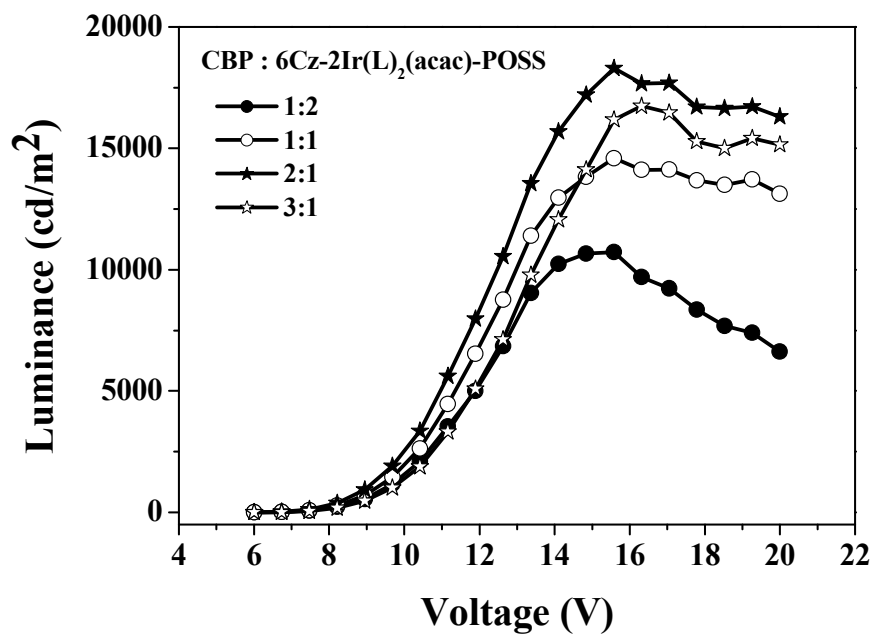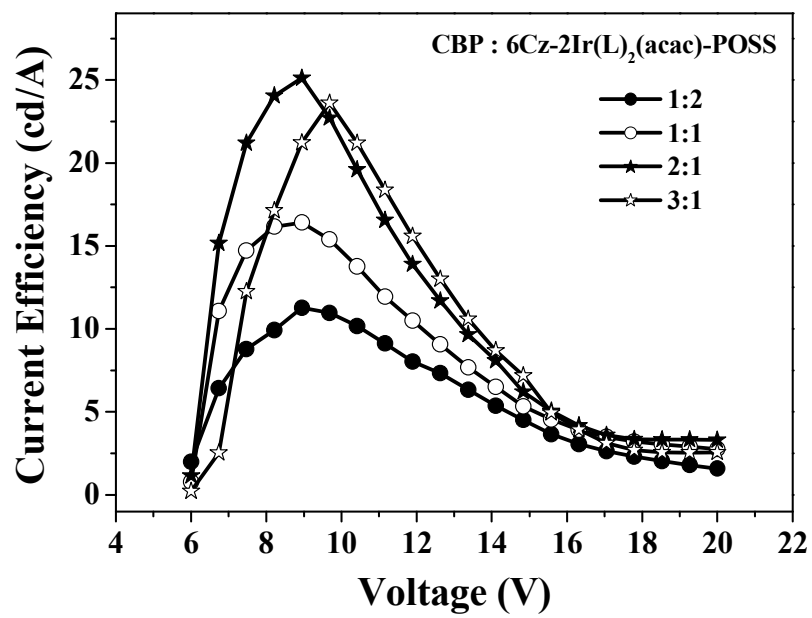
Table 1. Photophysical, thermal and electrochemical properties of the POSS materials

Material	UV-vis (nm)	PL (nm)	T_d (^{o}C)	τ (μs)	Φ_f (%)	$E_{1/2}^{OX}$ (V)	HOMO (eV)	LUMO (eV)
Ir(L)$_2$(acac-allyl)	227, 274, 345, 384, 438	530 567	352	9.22	9.15	1.11	-5.47	-2.84
7Cz-Ir(L)$_2$(acac)-POSS	236, 262, 295, 335, 346, 384, 440	530 567	373	9.27	9.43	0.88	-5.24	-2.59
6Cz-2Ir(L)$_2$(acac)-POSS	246, 262, 295, 335, 346, 384, 440	530 567	373	9.85	9.39	0.89	-5.25	-2.60

Table 2. EL performances of the POSS materials

CBP:POSS materials	V_{on} (V)	L_{max} (cd/m^2)	LE_{max} (cd/A)	EQE_{max} (%)
7Cz-Ir(L)$_2$(acac)-POSS				
1 : 2	6.3	18360@15.6 V	24.03@8.9 V	6.66
1 : 1	6.5	19530@15.6 V	28.22@8.9 V	7.82
2 : 1	6.6	16940@18.5 V	22.96@9.7 V	6.36
3 : 1	6.7	21285@19.3 V	23.46@11.2 V	6.50
4 : 1	6.6	19155@20.0 V	13.45@12.6 V	3.73
6 : 1	6.7	20895@18.5 V	11.76@15.6 V	3.26
8 : 1	6.5	18810@17.8 V	10.70@15.6 V	2.97
6Cz-2Ir(L)$_2$(acac)-POSS				
1 : 2	6.0	10725@15.6 V	11.28@8.9 V	3.13
1 : 1	6.2	14587@15.6 V	16.41@8.9 V	4.55
2 : 1	6.1	18300@15.6 V	25.12@8.9 V	6.96
3 : 1	6.3	16740@16.3 V	23.59@9.7 V	6.54